New Journal of Physics
The open access journal at the forefront of physics

Deutsche Physikalische Gesellschaft DPG IOP Institute of Physics

PAPER • OPEN ACCESS

Detection of HO_2 in an atmospheric pressure plasma jet using optical feedback cavity-enhanced absorption spectroscopy

To cite this article: Michele Gianella *et al* 2016 *New J. Phys.* **18** 113027

IOP Publishing New J. Phys. 18 (2016) 113027 doi:10.1088/1367-2630/18/11/113027

New Journal of Physics
The open access journal at the forefront of physics

Deutsche Physikalische Gesellschaft DPG
IOP Institute of Physics

Published in partnership with: Deutsche Physikalische Gesellschaft and the Institute of Physics

OPEN ACCESS

RECEIVED
18 August 2016

REVISED
26 October 2016

ACCEPTED FOR PUBLICATION
31 October 2016

PUBLISHED
16 November 2016

PAPER

Detection of HO_2 in an atmospheric pressure plasma jet using optical feedback cavity-enhanced absorption spectroscopy

Michele Gianella[1], **Stephan Reuter**[2], **Ana Lawry Aguila**[1], **Grant A D Ritchie**[1] **and Jean-Pierre H van Helden**[2]

[1] Department of Chemistry, Physical and Theoretical Chemistry Laboratory, University of Oxford, South Parks Rd, Oxford OX1 3QZ, UK
[2] Leibniz Institute for Plasma Science and Technology (INP Greifswald), Felix-Hausdorff-Str. 2, D-17489 Greifswald, Germany

E-mail: grant.ritchie@chem.ox.ac.uk

Keywords: atmospheric pressure plasma jet, optical feedback cavity-enhanced absorption spectroscopy, hydroperoxyl radical

Abstract

Cold non-equilibrium atmospheric pressure plasma jets are increasingly applied in material processing and plasma medicine. However, their small dimensions make diagnosing the fluxes of generated species a challenge. Here we report on the detection of the hydroperoxyl radical, HO_2, in the effluent of a plasma jet by the use of optical feedback cavity-enhanced absorption spectroscopy. The spectrometer has a minimum detectable absorption coefficient α_{min} of 2.25×10^{-10} cm^{-1} with a 100 second acquisition, equivalent to 5.5×10^{12} cm^{-3} of HO_2 (under ideal conditions). Concentrations in the range of $(3.1–7.8) \times 10^{13}$ cm^{-3} were inferred in the 4 mm wide effluent of the plasma jet.

1. Introduction

The hydroperoxyl radical, HO_2, plays an important role in atmospheric chemistry, as it is a key radical in the OH-induced oxidation cycle which controls virtually all of the daytime oxidative chemistry in the lower atmosphere and is therefore responsible for the transformation of primary emissions into secondary pollutants [1]. Furthermore, HO_2 is prevalent in hydrocarbon combustion [2-4] and in dielectric barrier discharges utilized for the purification of water [5] or the removal of volatile organic compounds in air [6].

The HO_2 radical is also considered to be an intrinsic part of the chemical reaction network in cold non-equilibrium atmospheric pressure plasmas, due to its involvement in the generation pathways of the hydroxy radical, OH, one of the most studied reactive species in plasma jets [7–11]. These plasma jets have gained strong attention over the past decade due to their use in the field of plasma medicine [12], where the high reactivity at low gas temperature is crucial for interaction with sensitive biological systems [11]. This makes them ideally suited for treatment of human tissue in plasma-assisted wound healing, cancer treatment [13], or sterilization [14]. The OH molecule is generated via pathways which include HO_2, which itself is quickly quenched by air derived species [10], and therefore HO_2 is mostly confined to the localized afterglow of the plasma jet. Due to their small size and high density gradients in space and time, these jets, however, are difficult to diagnose quantitatively. Absorption spectroscopy has become a popular method for characterizing the fluxes of species generated by these plasma sources [15]. To achieve space-resolved densities from the line-of-sight integrated densities, Abel inversion is most commonly used, which leads to a local density as a function of distance from the centre [16]. However, the generally small geometry of the effluent of a plasma jet (in μm to cm range) severely limits the sensitivity of the method, especially for highly reactive transient species.

To overcome the difficulty of small absorption lengths, cavity-enhanced spectroscopy is a promising method for localized measurements of species with low abundances in plasma jets. A wide class of cavity-enhanced spectroscopy techniques have been developed such as cavity ring-down spectroscopy (CRDS), off-axis cavity-enhanced absorption spectroscopy (CEAS), optical feedback cavity-enhanced absorption spectroscopy (OF-CEAS) and noise-immune cavity-enhanced optical heterodyne molecular spectroscopy (NICE-OHMS) [17, 18]. Of these variants, CRDS has been the method of choice for the detection of HO_2 utilizing absorption bands in the near-infrared (NIR) range [3, 19–21], although its detection using NICE-OHMS was also reported [22]. Similarly, CRDS has been employed for the detection of species in plasmas. An overview of the existing

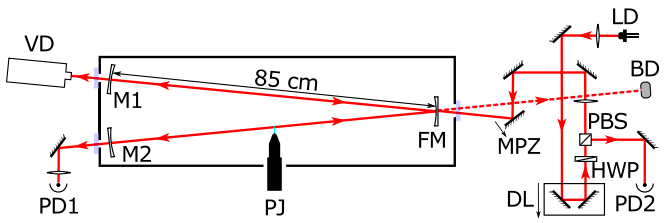

Figure 1. Schematic of the OF-CEAS experimental setup with the effluent of the atmospheric pressure plasma jet placed in one of the arms of the cavity. LD: laser diode; DL: delay line; HWP: half-wave plate; PBS: polarizing beam splitter; MPZ: mirror on piezo-electric transducer; FM: folding cavity mirror; M1, M2: cavity mirrors; VD: Vidicon camera; PD1, PD2: photodiodes; BD: beam dump; PJ: kINPen plasma jet device.

applications of CRDS to characterize various types of atmospheric pressure plasma jets can be found in [23]. In this paper, we utilize the related technique of OF-CEAS in which the laser is scanned over the spectral region of interest and locks, through optical feedback, to successive cavity resonances. Consequently, the optical cavity is used to both greatly increase the optical pathlength through the sample and enhance the measured signal intensity, resulting in very low detection limits being achievable [18, 24]. Initially, NIR diode lasers were used as sources [25, 26], but recently OF-CEAS instruments based on quantum and interband cascade lasers have also been reported [27–31].

Liu *et al* have measured the concentration of HO_2 in a dielectric barrier discharge plasma using NIR continuous wave (cw) CRDS and investigated the effect of water on the concentration of HO_2 in a $CH_2O/O_2/H_2O/N_2$ gas mixture [20]. These studies, however, were conducted at a pressure of 30 Torr and with a plasma sample length of 10 cm resulting in a detection limit of 1×10^{11} cm^{-3}. In this article, we present first measurements of HO_2 in the effluent of a mm size atmospheric plasma jet, the so-called kINPen-Sci, employing OF-CEAS using a diode laser at 1506.43 nm as the light source to probe HO_2 transitions in the the first vibrational overtone of the O–H stretch, the $2\nu_1$ band (centred at 6649 cm^{-1}). We begin our discussion by presenting the construction and performance of our OF-CEAS spectrometer.

2. Experimental setup

2.1. Laser spectrometer

Figure 1 is a schematic representation of the OF-CEAS spectrometer. The beam from a cw distributed feedback laser diode (LD, $\lambda = 1506.4$ nm, $P = 32$ mW, NTT Electronics NLK1S5D1TA) housed in a temperature-stabilized mount (Thorlabs TCLDM9) is collimated by a $f = 2.5$ mm lens and directed via protected silver mirrors (Thorlabs PF10-03-P01) to a delay line (DL), a half-wave plate (HWP, Thorlabs WPH05M-1310), a polarizing beam splitter (PBS, Thorlabs PBS104), and into the V-shaped cavity. Current and temperature of the laser are controlled by two modules (Thorlabs LDC8002 and TEC8020) housed in a chassis (Thorlabs PRO8000). The polarization axis of the linearly polarized beam can be rotated with the HWP (mounted in a rotation mount, Thorlabs RSP1), so that the intensity ratio between the transmitted and reflected beams after the PBS can be adjusted. The intensity of the beam reflected by the PBS is measured by an InGaAs photodiode (PD2, Thorlabs DET410). After the PBS, a mode-matching lens with $f = 500$ mm (Thorlabs LA1908-C) focuses the beam to the waist size and position required to excite the fundamental transverse cavity mode. The last mirror before the cavity (MPZ) is mounted on a piezo-electric transducer. The piezo-mounted mirror and the DL allow for fine and coarse adjustment of the distance between the laser diode and the folding mirror (FM) of the cavity. The optical cavity consists of three highly reflective dielectric mirrors (Layertec) with an effective reflectivity > 0.9999, arranged in a V shape with an angle of 5.5° and an arm length of 85 cm. The external reflection off the FM is collected by a beam dump (BD). A Vidicon camera (VD, Electrophysics MicronViewer 7290A) placed at one of the output ports allows monitoring of the beam profile, while an InGaAs photodiode (PD1, Thorlabs DET10C/M) measures the transmitted intensity through the cavity. A transimpedance amplifier (Femto DLPCA-200) with the gain typically set to 10^6 V A^{-1} amplifies the photocurrent from PD1 prior to digitization by a USB data acquisition module (National Instruments NI-USB 6356). The signal from PD2 does not require amplification. The spectrometer is controlled by a custom LabVIEW (National Instruments) program running on a standard PC. The beam in one of the arms of the V-shaped cavity intercepts the effluent from a kINPen plasma jet device (PJ). The cavity is enclosed by an aluminium box with inner dimensions of $93 \times 23 \times 15$ cm (width$\times$depth $\times$height) and an acrylic glass lid.

The theoretical framework of optical feedback-based spectrometers and their advantages are described in detail elsewhere (see for example [18], chapter 5), so the working principle will only be outlined briefly here.

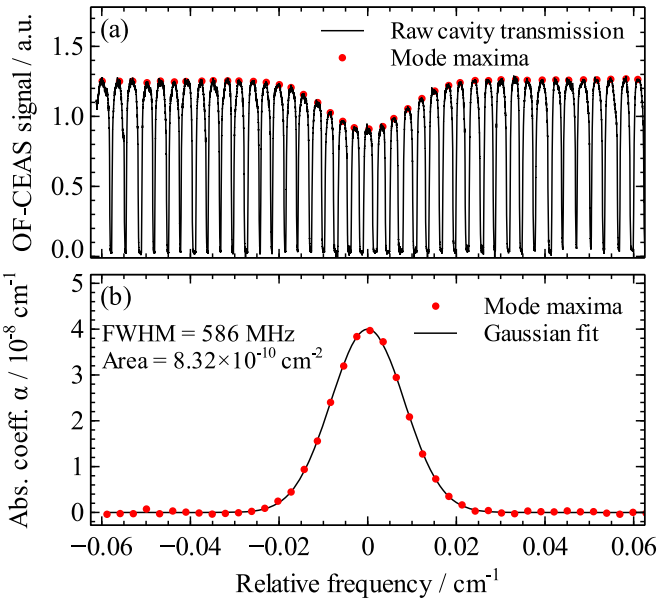

Figure 2. (a) Raw cavity transmission and mode maxima for $p < 0.1$ mbar of lab air. A water absorption line ($\lambda = 1504.740$ nm, $S = 1.743 \times 10^{-23}$ cm^2 cm^{-1} molecule^{-1}) is visible. (b) Corresponding absorption coefficient spectrum computed with equation (3) together with a Gaussian fit.

Optical feedback techniques exploit the very strong response of a diode laser to radiation intentionally allowed to return to it. Under appropriate conditions, when radiation returns from a high-finesse cavity to the laser source, optical feedback can: (a) significantly reduce the emission linewidth of the laser, e.g., from MHz to below 1 kHz, thus increasing the throughput and the coupling efficiency of the laser with the cavity; (b) lock the emission frequency of the laser to a cavity resonance. As the laser frequency is scanned (by ramping its current or temperature), the laser locks to successive cavity modes, ideally with little or no time period during which the laser is free-running ('unlocked'). This behaviour is illustrated in figure 2(a), where the black trace shows the raw cavity transmission spectrum. A weak water transition is present in the measured frequency interval.

One of the parameters that plays an important role in the context of optical feedback is the exact distance between the laser facet and the entry mirror of the cavity (the folding mirror in a V-shaped cavity). In order for optical feedback to successfully lock the laser emission frequency to any cavity mode, the distance D between the laser facet and the entry mirror must be equal to $D = L_2 + q(L_1 + L_2)$, where L_1 is the injection arm length (FM-M1 in figure 1), L_2 is the arm length FM-M2, and $q \geqslant 0$ is an integer [18]. In our case, $q = 0$ and $D = L_2 = 85$ cm. It can be shown that the shape of the modes (see black trace in figure 2(a)) depends on this condition being fulfilled. When that is the case, the modes have a roughly symmetric appearance, but when $D \neq L_2$ they become more and more asymmetric, depending on the sign of $D - L_2$ [32]. This asymmetry is used here as an error signal to maintain the distance D at its correct value: an average asymmetry value is computed for the modes in each scan, and this value is then used to adjust the voltage applied on the piezo (MPZ in figure 1).

2.2. Extraction of quantitative data

The transmission maximum of each mode can be evaluated from the transfer function of a V-shaped cavity at the kth resonance [18]:

$$H_k \approx \left[\frac{T}{1 - R^2 \exp(-\alpha_k L)}\right]^2 = \left[\frac{T}{1 - \exp(-\tilde{\alpha}_k L)}\right]^2, \quad (1)$$

where T and R are the mirror (intensity) transmission and reflection coefficients, L is the sum of the two arm lengths of the cavity, and $\tilde{\alpha}_k = \alpha_k - 2L^{-1} \ln R$ is termed the *equivalent* absorption coefficient of the cavity (assuming the mirror's contribution to the cavity losses to be distributed over the length of the cavity). Equation (1) can be solved with respect to $\tilde{\alpha}_k$ to yield

$$\tilde{\alpha}_k = \frac{T}{L\sqrt{H_k}} = \frac{1}{c\tau_k}. \quad (2)$$

The maximum H_k of each mode is extracted experimentally from the raw cavity transmission (red circles in figure 2(a)). The second equality in equation (2) exploits the relationship between the ring-down time τ and the

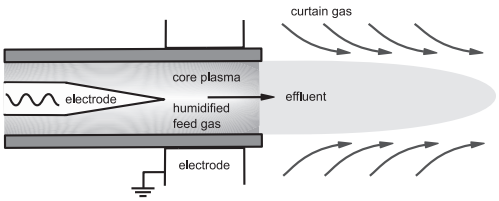

Figure 3. Schematic of the plasma jet operated with 1 MHz excitation frequency and a feed gas flow of 3 slm argon. The gas curtain is operated with synthetic air. A bubbler system and a hygrometer allow for controlled humidification of the feed gas [36, 37].

cavity losses $\tilde{\alpha}$. By abruptly detuning the laser from the last mode n of the cavity, a ring-down event is induced from which the ring-down time τ_n can be extracted. By also measuring the amplitude H_n of this mode, the factor T/L in equation (2) can be determined, $T/L = \sqrt{H_n}/(c\tau_n)$, yielding:

$$\tilde{\alpha}_k = \frac{1}{c\tau_n}\sqrt{\frac{H_n}{H_k}}. \tag{3}$$

To obtain α_k, the mirror-losses term $(-2L^{-1}\ln R)$ must be accounted for, either through a zero-absorption measurement (where $\alpha = 0$ and therefore $\tilde{\alpha} = -2L^{-1}\ln R$), or through fitting a baseline to $\tilde{\alpha}$. Here, we always employed the second approach.

From the mode amplitudes in figure 2(a) the equivalent absorption coefficient is computed with equation (3) and is shown in figure 2(b). The feature shown is a water absorption line located at 1504.740 nm measured at a pressure $p < 0.1$ mbar with an integrated absorption cross-section of $S = 1.743 \times 10^{-23}$ cm^2 cm^{-1} molecule^{-1} (($\nu_1\ \nu_2\ \nu_3$) = (0 0 0) → (0 2 1), ($J\ K_a\ K_c$) = (5 3 2) → (4 1 3)). The relationship between absorption cross-section σ and absorption coefficient α, $\alpha = N\sigma$, can be used to extract the number density of the absorber, N, from the integrated absorption coefficient:

$$N = \frac{\int \alpha(\nu)\,\mathrm{d}\nu}{\int \sigma(\nu)\,\mathrm{d}\nu} = \frac{A}{S}, \tag{4}$$

where S is the line strength (or integrated absorption cross-section) and A is the integrated absorption coefficient. For the water absorption line in figure 2 we obtain $N = 4.8 \times 10^{13}$ cm^{-3}. The measured full width at half maximum (FWHM) of 586 ± 3 MHz is close to the theoretical value of 580 MHz at 298 K. As the frequency axis in figure 2 is determined via the free spectral range of the cavity, which in turn is computed from the measurement of the two arm lengths, the small discrepancy in width could be explained by an error in the cavity length measurement.

2.3. Plasma jet

The non-thermal plasma used to generate the HO_2 is an argon atmospheric pressure plasma jet operated at a radio frequency around 1 MHz (figure 3). The so-called kINPen-Sci has a pin type powered electrode centred in a dielectric tubing with a circular grounded electrode outside the dielectric [33]. The plasma jet is operated at about 1 W dissipated plasma power. The energy is quickly transferred to metastable states of argon or nitrogen [10, 34]. The plasma jet is equipped with a gas curtain device which allows control of the atmosphere surrounding its active afterglow [35]. Changing the composition of the curtain gas strongly influences the reactive component composition generated by the plasma. For instance, humidity variation controls the output of H_2O_2 and OH [36]. The plasma jet is introduced into the cavity via a side opening. An xy-stage allowed a precise positioning of the effluent of the plasma jet to intersect the laser beam. The laser beam of 1 mm diameter passed through the plasma effluent at 11 mm distance from the plasma jet's nozzle as this is the typical distance between plasma jet and treated surfaces. The feed gas argon has a flow rate of 3 standard litre per minute (slm) through the plasma jet. It is humidified by passing a small fraction (4%–10%) through a water bubbler held at room temperature. The feed gas humidity is measured with a chilled mirror dew point hygrometer (EdgeTech DewMaster) according to the procedure described previously [36]. The gas curtain is operated with a mixture of 20% oxygen (purity 2.6) to 80% nitrogen (purity 4.8) at a flow rate of 5 slm. All gas flows are controlled via electronic mass flow controllers (MKS Instruments).

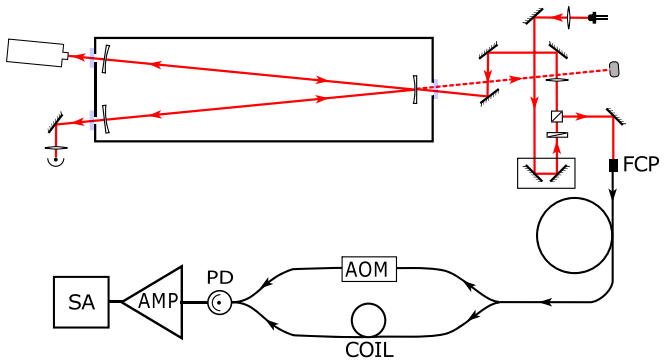

Figure 4. Delayed self-heterodyne setup used for the linewidth measurements. FCP: fibre collimation package; AOM: acousto-optic modulator; PD: photodiode; AMP: amplifier; SA: spectrum analyzer.

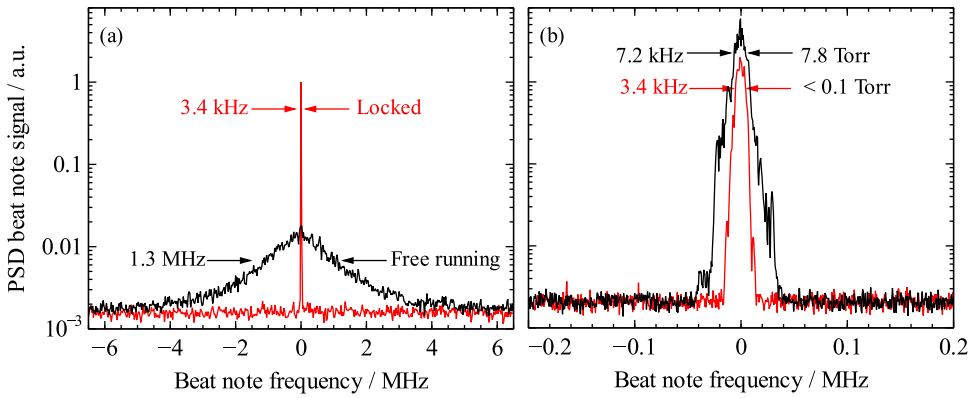

Figure 5. Power spectral density (PSD) of the beat note signal obtained with a delayed self-heterodyne measurement. (a) Free-running ('unlocked') and cavity-locked laser. (b) Cavity-locked in both cases with the cell under vacuum and with 7.8 Torr of air. Notice the different frequency axes in both figures.

3. Results

3.1. Performance of the OF-CEAS spectrometer

3.1.1. Laser linewidth

The data points in all the absorption spectra presented here are spaced by the free spectral range of the cavity, 88.4 MHz, while the laser linewidth—with ring-down times ranging from 130 to 150 μs—is expected to be of the order of $(2\pi\tau)^{-1} \approx 1$ kHz. Indeed, measurements taken with a delayed self-heterodyne setup (figure 4) confirm this supposition and show how the cavity losses affect the laser linewidth. The delayed self-heterodyne system was based on the conventional design where an acousto-optic modulator (AOM, Gooch & Housego FibreQ) and a fibre coil are employed to frequency-shift (80 MHz) and time-delay ($\tau_d = 5$ μs), respectively, the waves propagating in the two arms of a fibre interferometer [38]. The beam was coupled into the fibre via a fibre collimation package (FCP) placed instead of the reference detector (PD2 in figure 1). After recombination of the two arms of the fibre interferometer, a fast photodiode (PD, Hamamatsu G8372-01), transimpedance amplifier (AMP, FEMTO DHPCA-100), and a spectrum analyzer (SA, HP 8560E) measure the beat note signal.

Assuming white phase noise and $\tau_d \gg \tau_c$, where τ_c is the coherence time of the beam, the power spectral density (PSD) of the beat note signal has the same (Lorentzian) shape as the laser emission spectrum, but with a width twice as large [38]. The free-running laser exhibits a linewidth of 1.3 MHz, which reduces to 3.4 kHz when the laser is locked to the cavity (figure 5(a)). The condition $\tau_d \gg \tau_c$ is fulfilled in the free-running case ($\tau_c < 1$ μs), when the beam is blocked between the mode-matching lens and the cavity, but not in the case with optical feedback. For this reason, the linewidth of 3.4 kHz quoted above is not accurate. A better value could be obtained by modelling the PSD of the beat note signal, for example as in equation (17) in [38], but this is beyond the scope of this article. Nevertheless, the effect of optical feedback on the laser emission spectrum is evident from figure 5(a), at least qualitatively. The reduced linewidth dramatically increases the coupling efficiency between laser and high-finesse cavity and is one of the advantages of OF-CEAS.

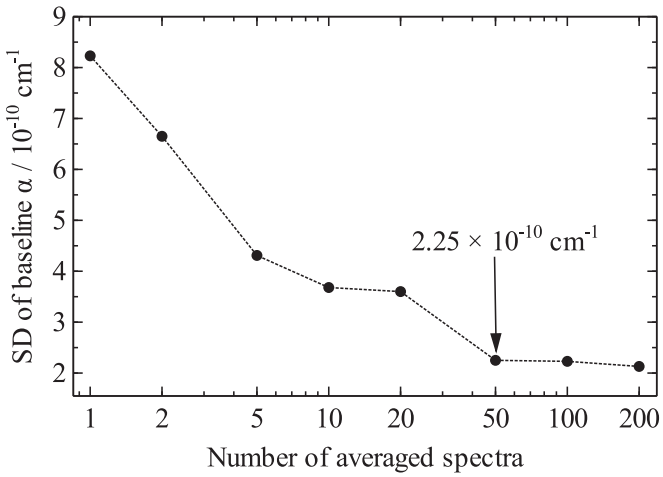

Figure 6. Standard deviation (SD) of baseline noise as a function of number of averaged spectra.

Allowing 7.8 Torr of air into the cavity reduces its finesse due to absorption of the laser light by the water continuum. The increase in cavity losses is measurable as a decrease in ring-down time or, equivalently, as a broadening of the cavity resonance width and, through optical feedback, of the laser linewidth. This phenomenon is clearly visible in figure 5(b), where the PSD of the beat note signal is shown under conditions of vacuum ($p < 0.1$ Torr) and with 7.8 Torr of air. Again, as the condition $\tau_d \gg \tau_c$ is not fulfilled, the quoted linewidths are not accurate. In figure 5(b) we merely aim to show the qualitative increase in laser linewidth due to larger cavity losses.

3.1.2. Sensitivity

A typical scan covers about 270 modes or 24 GHz (0.8 cm^{-1}) and takes 2 s to complete. There is a short dead time of about 0.25 s after each scan to compute the error signal needed for the laser-to-cavity distance adjustment. The acquisition rate is about 0.44 s^{-1} or 800 spectra in 30 min. By averaging multiple spectra together, noise can be reduced at the expense of a longer measurement time. We define the *baseline noise* as the standard deviation (SD) of the absorption coefficient α measured over a region free of absorption. Figure 6 shows the SD of α as a function of the number of spectra averaged together. Averaging more than about 50 scans does not significantly reduce the noise but simply increases the duration of the measurement. With 50 averaged spectra, the entire series can be acquired in 100 s, and the SD of α is $\alpha_{min} = 2.25 \times 10^{-10}$ cm^{-1}.

We can then estimate the limit of detection (LOD) for HO_2 by assuming the smallest absorption we can reliably detect to be $\alpha_{min} = 2.25 \times 10^{-10}$ cm^{-1} and exploiting

$$N_{min} = \frac{\alpha_{min}}{\sigma_p} \approx \frac{\pi \Gamma \alpha_{min}}{2S} \approx 1.3 \times 10^{10}\ cm^{-3} = 0.52\ ppb, \quad (5)$$

where σ_p is the peak absorption cross-section, Γ is the FWHM ($\Gamma \approx 0.23$ cm^{-1} [39]), and $S = (\pi/2)\sigma_p\Gamma$ is the line strength of the HO_2 absorption feature ($S = 9.61 \times 10^{-21}$ cm^2 cm^{-1} $molecule^{-1}$); the factor $\pi/2$ arises from the lineshape, which we assume to be Lorentzian. The value of N_{min} in equation (5) assumes that absorption is homogeneous along the full length (1.7 m) of the cavity.

In order to determine absolute concentrations of the HO_2 radicals in the plasma jet, an assumption has to be made on the pathlength over which the radicals absorb. From quantitative schlieren diagnostics on the plasma jet an absorption length of 4 mm for the plasma effluent at 11 mm distance from the plasma jet's nozzle was obtained [16]. In our calculations we also assume a homogeneous concentration distribution of the radicals over the absorption pathlength. If the absorption is confined to a 4 mm region, the LOD increases by a factor 1.7 m/4 mm = 425 to $N_{min} = 5.5 \times 10^{12}$ cm^{-3}. This LOD is valid for a zero flow in the cavity. When the kINPen device is active, however, the gas flow and the discharge cause very strong fluctuations in the cavity transmission, and the LOD worsens. The turbulent gas flow destroys the coherence of the optical system and makes the optical power build-up within the cavity more sporadic [40]. A very large number of spectra must then be acquired, most of which have to be discarded because of excessive noise or loss of frequency locking. In the following measurements, we typically acquired 800 spectra (30 min), of which only 200–300 were usable and averaged together.

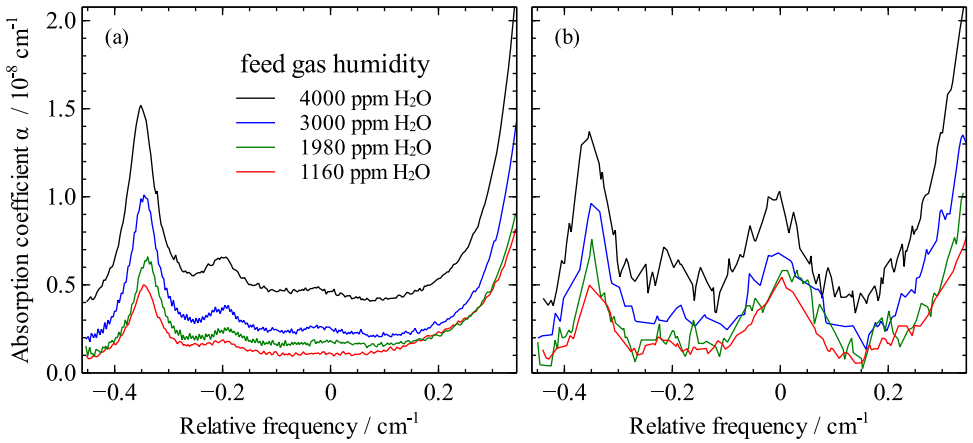

Figure 7. Absorption spectra for four values of the feed gas humidity. (a) Without plasma. (b) With plasma. The vertical scales are identical.

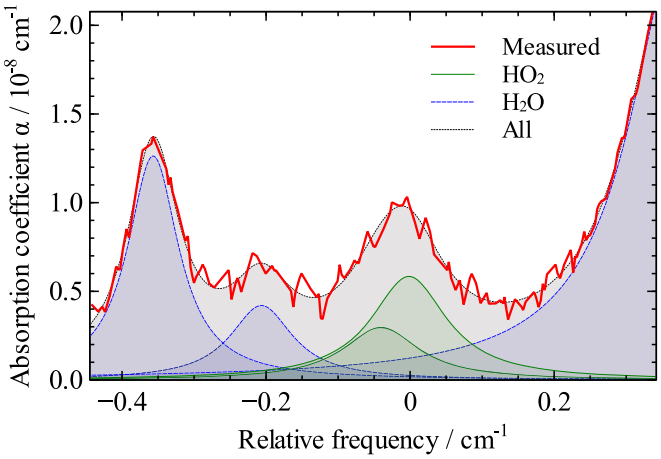

Figure 8. Absorption coefficient spectrum for a water admixture of 4000 ppm to the Ar feed gas with a composite fit taking into account the two HO_2 and three H_2O transitions which contribute to the observed absorption features.

3.2. HO_2 spectroscopy and relationship between H_2O and HO_2

The absorption feature of HO_2 selected for the investigation in this work consists primarily of two transitions assigned by DeSain *et al* [41] as the $^qP_0(6)$ transition at 6638.11 cm^{-1}, consisting of two transitions due to spin-rotation splitting, and the overlapping $^qQ_3(N)$ transitions with $N = 4$–9 at 6638.20 cm^{-1}, consisting each time of two transitions due to spin-rotation splitting. The Doppler-limited peak absorption cross-section (at zero pressure) for the latter transition was reported at 296 K to be 4.2×10^{-19} cm^2 $molecule^{-1}$ by Thiebaud *et al* [19] and $(4.3 \pm 1.1) \times 10^{-19}$ cm^2 $molecule^{-1}$ by Tang *et al* [21]. Given the Doppler width at 296 K, this corresponds to a linestrength S of 6.37×10^{-21} cm^2 cm^{-1} $molecule^{-1}$ for the transition at 6638.20 cm^{-1}. From the ratio of cross-sections between this transition and the transition at 6638.11 cm^{-1} measured in 50 Torr of He, both having the same FWHM, we calculated a S of 3.23×10^{-21} cm^2 cm^{-1} $molecule^{-1}$ for the latter transition. Therefore, the total linestrength of the composite absorption feature of HO_2 is $S = 9.61 \times 10^{-21}$ cm^2 cm^{-1} $molecule^{-1}$.

In figure 7, the measured spectra for four different feed gas humidities without and with the plasma switched on are shown. The water concentration was determined by a dew point measurement and is rounded to 10 s of ppm. We did not deduce the water concentration from the measured absorptions since these are due not only to the water in the plasma jet, but also to water absorbing along the full length (1.7 m) of the cavity (the optical cavity is open to laboratory air). HO_2, on the other hand, being quickly quenched by air derived species, does not diffuse within the cell but is localized in the jet region. With the plasma switched off, the measured absorption spectrum is due to three water transitions at 6637.850 cm^{-1}, 6637.995 cm^{-1}, and 6638.573 cm^{-1} [42]; these are centred at relative frequencies of -0.355 cm^{-1}, -0.210 cm^{-1}, and 0.368 cm^{-1}, respectively. With the plasma switched on, the HO_2 absorption feature, centred at 0 cm^{-1} relative frequency, appears. As can be seen, the

'plasma on' spectrum is much noisier due to the plasma disturbing the stability of the cavity. A composite fit to the absorption features for a feed gas humidity of 4000 ppm is shown in figure 8. As the measurements were performed at atmospheric pressure, to obtain the area under the HO_2 absorption feature (the integrated absorption in equation (4)), the absorption spectra were fitted to five Lorentzian profiles. The absorption feature for HO_2 was fitted by a double Lorentzian with the relative centre frequencies and areas fixed and the same Lorentzian linewidth for both. The water transitions were also included to account for their overlap with HO_2. The HO_2 concentrations as the feed gas humidity was changed from 1000 to 4000 ppm were in the range of (3.1 ± 0.3)–$(7.8 \pm 1.0) \times 10^{13}$ cm^{-3}. The main uncertainty in the determination of these concentrations is the absorption pathlength of 4 mm for the plasma effluent at 11 mm distance from the plasma jet's nozzle. The number densities are in broad agreement with predictions from modelling of these plasmas [10]. We note, however, that such cavity-based measurements provide a new way of testing and improving our modelling of these complex environments.

4. Conclusion

In summary, we have presented an OF-CEAS experiment and demonstrated its first application to the detection of HO_2 in the effluent of a plasma jet. We demonstrated a sensitivity of 2.25×10^{-10} cm^{-1} with a 100 seconds acquisition time under ideal conditions, which translates into a sensitivity of 5.5×10^{12} cm^{-3} of HO_2 assuming an absorption length of 4 mm. In the plasma jet, HO_2 concentrations in the range of $(3.1–7.8) \times 10^{13}$ cm^{-3} were detected. The detection levels indicate that such a spectrometer will find broad application in future studies of the chemical network in the effluents of plasma jets.

Acknowledgments

The authors gratefully acknowledge Dr Luca Ciaffoni for help in carrying out the linewidth measurements. This work was funded by: Leibniz Competition 2015 (SAW-2015-INP-5); Ministry of Education, Science and Culture of the State of Mecklenburg-Vorpommern (AU 15001); European Union Seventh Framework Programme FP7/2007-2013 (316216); Natural Environment Research Council (NERC) (NE/M016439/1).

References

[1] Heard D and Pilling M J 2003 Measurement of OH and HO_2 in the troposhere *Chem. Rev.* **103** 5163–98
[2] Blocquet M, Schoemaecker M, Amedro D, Herbinet O, Battin-Leclerc F and Fittschen C 2013 Quantification of OH and HO_2 radicals during the low-temperature oxidation of hydrocarbons by fluorescence assay by gas expansion technique *Proc. Natl Acad. Sci. USA* **110** 20014–7
[3] Djehiche M, Tan N L L, Jain C D, Dayma G, Dagaut P, Chauveau C, Pillier L and Tomas A 2014 Quantitative measurements of HO_2 and other products of n-butane oxidation (H_2O_2, H_2O, CH_2O, and C_2H_4) at elevated temperatures by direct coupling of a jet-stirred reactor with sampling nozzle and cavity ring-down spectroscopy (CW-CRDS) *J. Am. Chem. Soc.* **136** 16689–94
[4] Brumfield B, Sun W, Ju Y and Wysocki G 2013 Direct *in situ* quantification of HO_2 from a flow reactor *J. Phys. Chem. Lett.* **4** 872–6
[5] Malik M A, Ghaffar A and Malik S A 2001 Water purification by electrical discharges *Plasma Sources Sci. Technol.* **10** 82–91
[6] Blin-Simiand N, Pasquiers P and Magne L 2016 Removal of formaldehyde by a pulsed dielectric barrier discharge in dry air in the 20°C–300 °C temperature range *J. Phys. D: Appl. Phys.* **49** 195202
[7] Tresp H, Hammer M U, Winter J, Weltmann K-D and Reuter S 2013 Quantitative detection of plasma-generated radicals in liquids by electron paramagnetic resonance spectroscopy *J. Phys. D: Appl. Phys.* **46** 435401
[8] Norberg S A, Tian W, Johnsen E and Kushner M J 2014 Atmospheric pressure plasma jets interacting with liquid covered tissue: touching and not-touching the liquid *J. Phys. D: Appl. Phys.* **47** 475203
[9] Gaens W V and Bogaerts A 2013 Kinetic modelling for an atmospheric pressure argon plasma jet in humid air *J. Phys. D: Appl. Phys.* **46** 275201
[10] Schmidt-Bleker A, Winter J, Bösel A, Reuter S and Weltmann K-D 2016 On the plasma chemistry of a cold atmospheric argon plasma jet with shielding gas device *Plasma Sources Sci. Technol.* **25** 015005
[11] Lu X, Naidis G V, Laroussi M, Reuter S, Graves D B and Ostrikov K 2016 Reactive species in non-equilibrium atmospheric-pressure plasmas: generation, transport, and biological effects *Phys. Rep.* **630** 1–84
[12] von Woedtke T, Reuter S, Masur K and Weltmann K-D 2013 Plasmas for medicine *Phys. Rep.* **530** 291–320
[13] Yan D, Sherman J H, Cheng X, Ratovitski E, Canady J and Keidar M 2014 Controlling plasma stimulated media in cancer treatment application *Appl. Phys. Lett.* **105** 224101
[14] Nagatsu M, Terashita F, Nonaka H, Xu L, Nagata T and Koide Y 2005 Effects of oxygen radicals in low-pressure surface-wave plasma on sterilization *Appl. Phys. Lett.* **86** 211502
[15] Reuter S, Sousa J S, Stancu G D and van Helden J-P H 2015 Review on VUV to MIR absorption spectroscopy of atmospheric pressure plasma jets *Plasma Sources Sci. Technol.* **24** 054001
[16] Schmidt-Bleker A, Reuter S and Weltmann K-D 2015 Quantitative schlieren diagnostics for the determination of ambient species density, gas temperature and calorimetric power of cold atmospheric plasma jets *J. Phys. D: Appl. Phys.* **48** 175202
[17] Berden G and Engeln R 2009 *Cavity Ring-Down Spectroscopy: Techniques and Applications* (Oxford: Wiley-Blackwell)
[18] Gagliardi G and Loock H-P 2014 *Cavity-Enhanced Spectroscopy and Sensing* (Berlin: Springer)

[19] Thiebaud J, Crunaire S and Fittschen C 2007 Measurements of line strengths in the $2\nu_1$ band of the HO_2 radical using laser photolysis/continuous wave cavity ring-down spectroscopy (CW-CRDS) *J. Phys. Chem.* A **111** 6959–66
[20] Liu Z W, Xu Y, Yang X F, Zhu A M, Zhao G L and Wang W G 2008 Determination of the HO_2 radical in dielectric barrier discharge plasmas using near-infrared cavity ring-down spectroscopy *J. Phys. D: Appl. Phys.* **41** 045203
[21] Tang Y, Tyndall G S and Orlando J J 2010 Spectroscopic and kinetic properties of HO_2 radicals and the enhancement of the HO_2 self reaction by CH_3OH and H_2O *J. Phys. Chem.* A **114** 369–78
[22] Bell C L, van Helden J-P H, Blaikie T P J, Hancock G, van Leeuwen N J, Peverall R and Ritchie G A D 2012 Noise-immune cavity-enhanced optical heterodyne detection of HO_2 in the near-infrared range *J. Phys. Chem.* A **116** 5090
[23] Zaplotnik R, Bišćan M, Krstulović N, Popović D and Milošević S 2015 Cavity ring-down spectroscopy for atmospheric pressure plasma jet analysis *Plasma Sources Sci. Technol.* **24** 054004
[24] Morville J, Kassi S, Chenevier M and Romanini D 2005 Fast, low-noise, mode-by-mode, cavity-enhanced absorption spectroscopy by diode-laser self-locking *Appl. Phys.* B **80** 1027–38
[25] Romanini D, Chenevier M, Kassi S, Schmidt M, Valant C, Ramonet M, Lopez J and Jost H-J 2006 Optical-feedback cavity-enhanced absorption: a compact spectrometer for real-time measurement of atmospheric methane *Appl. Phys.* B **83** 659–67
[26] Baran S G, Hancock G, Peverall R, Ritchie G A D and van Leeuwen N J 2009 Optical feedback cavity enhanced absorption spectroscopy with diode lasers: a sensitive tool for environmental and medical detection *Analyst* **134** 243–9
[27] Maisons G, Gorrotxategi-Carbajo P, Carras M and Romanini D 2010 Optical-feedback cavity-enhanced absorption spectroscopy with a quantum cascade laser *Opt. Lett.* **35** 3607–9
[28] Hamilton D J and Orr-Ewing A J 2011 A quantum cascade laser-based optical feedback cavity-enhanced absorption spectrometer for the simultaneous measurement of CH_4 and N_2O in air *Appl. Phys.* B **102** 879–90
[29] Bergin A G V, Hancock G, Ritchie G A D and Weidmann D 2013 Linear cavity optical-feedback cavity-enhanced absorption spectroscopy with a quantum cascade laser *Opt. Lett.* **38** 2475–7
[30] Manfred K M, Ritchie G A D, Lang N, Röpcke J and van Helden J-P H 2015 Optical feedback cavity-enhanced absorption spectroscopy with a 3.24 μm interband cascade laser *Appl. Phys. Lett* **106** 221106
[31] Lang N, Macherius U, Wiese M, Zimmermann H, Röpcke J and van Helden J-P H 2016 Sensitive CH_4 detection applying quantum cascade laser based optical feedback cavity-enhanced absorption spectroscopy *Opt. Express* **24** A536–43
[32] Habig J C, Nadolny J, Meinen J, Saathoff H and Leisner T 2012 Optical feedback cavity enhanced absorption spectroscopy: effective adjustment of the feedback-phase *Appl. Phys.* B **106** 491–9
[33] Dünnbier M, Schmidt-Bleker A, Winter J, Wolfram M, Hippler R, Weltmann K-D and Reuter S 2013 Ambient air particle transport into the effluent of a cold atmospheric-pressure argon plasma jet investigated by molecular beam mass spectrometry *J. Phys. D: Appl. Phys.* **46** 435203
[34] Iseni S, Bruggeman P J, Weltmann K-D and Reuter S 2016 Nitrogen metastable (N_2 ($A^3\Sigma_u^+$)) in a cold argon atmospheric pressure plasma jet: shielding and gas composition *Appl. Phys. Lett.* **108** 184101
[35] Reuter S, Tresp H, Wende K, Hammer M U, Winter J, Masur K, Schmidt-Bleker A and Weltmann K-D 2012 From RONS to ROS: tailoring plasma jet treatment of skin cells emph *IEEE Trans. Plasma Sci.* **40** 2986–93
[36] Winter J *et al* 2014 Tracking plasma generated H_2O_2 from gas into liquid phase and revealing its dominant impact on human skin cells *J. Phys. D: Appl. Phys.* **47** 285401
[37] Reuter S, Winter J, Schmidt-Bleker A, Tresp H, Hammer M U and Weltmann K-D 2012 Controlling the ambient air affected reactive species composition in the effluent of an argon plasma jet *IEEE Trans. Plasma Sci.* **40** 2788–94
[38] Han M and Wang A 2005 Analysis of a loss-compensated recirculating delayed self-heterodyne interferometer for laser linewidth measurement *Appl. Phys.* B **81** 53
[39] Ibrahim N, Thiebaud J, Orphal J and Fittschen C 2007 Air-broadening coefficients of the HO_2 radical in the $2\nu_1$ band *J. Mol. Spectrosc.* **242** 64–9
[40] Iseni S, Schmidt-Bleker A, Winter J, Weltmann K-D and Reuter S 2014 Atmospheric pressure streamer follows the turbulent argon air boundary in a MHz argon plasma jet investigated by OH-tracer PLIF spectroscopy *J. Phys. D: Appl. Phys.* **47** 152001
[41] DeSain J D, Ho A D and Taatjes C A 2003 High-resolution diode laser absorption spectroscopy of the O–H stretch overtone band (2,0,0) ← (0,0,0) of the HO_2 radical *J. Mol. Spectrosc.* **219** 163–9
[42] Rothman L S *et al* 2013 The HITRAN2012 molecular spectroscopic database *J. Quant. Spectrosc. Radiat. Transfer* **130** 4–50